PHYSIOLOGY

# High-fat feeding drives the intestinal production and assembly of $C_{16:0}$ ceramides in chylomicrons

**Michael SM Mah[1], Enyuan Cao[1], Dovile Anderson[1], Alistair Escott[2,3], Surafel Tegegne[1], Gracia Gracia[1], Joel Schmitz[4], Susanne Brodesser[5], Colby Zaph[6], Darren J. Creek[1], Jiwon Hong[2,7], John A. Windsor[2,3], Anthony RJ Phillips[2,7], Natalie L. Trevaskis[1], Mark A. Febbraio[1]*, Sarah M. Turpin-Nolan[1]***



**Consumption of a diet rich in saturated fat increases lipid absorption from the intestine, assembly into chylomicrons, and delivery to metabolic tissues via the lymphatic and circulatory systems. Accumulation of ceramide lipids, composed of sphingosine and a fatty acid, in metabolic tissues contributes to the pathogenesis of cardiovascular diseases, type 2 diabetes mellitus and cancer. Using a mesenteric lymph duct cannulated rat model, we showed that ceramides are generated by the intestine and assembled into chylomicrons, which are transported via the mesenteric lymphatic system. A lipidomic screen of intestinal-derived chylomicrons identified a diverse range of fatty acid, sphingolipid, and glycerolipid species that have not been previously detected in chylomicrons, including the metabolically deleterious $C_{16:0}$ ceramide that increased in response to high-fat feeding in rats and human high-lipid meal replacement enteral feeding. In conclusion, high-fat feeding increases the export of intestinal-derived $C_{16:0}$ ceramide in chylomicrons, identifying a potentially unknown mechanism through which ceramides are transported systemically to contribute to metabolic dysfunction.**

## INTRODUCTION

Ceramide lipid accumulation during obesity is strongly associated with insulin resistance and metabolic dysfunction (*1*–*4*). Overconsumption of a diet rich in saturated fat markedly enriches the key dietary constituents palmitoyl–coenzyme A and serine, which are the two requisite components for de novo ceramide synthesis within the sphingolipid pathway. The de novo sphingolipid pathway is the most important route of ceramide biosynthesis and is a unidirectional arm that directly contributes to the central ceramide pool [for a more in-depth review, refer to (*5*)]. Increases in circulating and intracellular ceramide content have been observed in both obese humans and rodents. However, the mechanistic links associated with metabolic dysfunction is dependent on the manipulation of ceramides, or lack thereof, with different fatty acyl moieties attached by ceramide synthase enzymes during de novo synthesis (*5*–*7*). The liver, particularly, has been a primary focal point for research investigating the link between ceramide metabolism and metabolic disease due to its enhanced capacity for lipid uptake and redistribution to peripheral metabolic tissues (*1*, *8*, *9*). During obesity, metabolically pathogenic $C_{16:0}$ ceramide species accumulate in the liver and visceral adipose tissue depots (*1*, *3*). $C_{16:0}$ ceramide–driven metabolic dysfunction occurs via inhibition of hepatic and brown adipose tissue mitochondrial β-oxidation. Therefore, reducing hepatic $C_{16:0}$ ceramides increases mitochondrial lipid utilization in the liver and restores glucose tolerance in mice (*1*, *9*). The deleterious action of specific ceramide species in other key metabolic organs such as skeletal muscle has also been linked to the development of obesity-associated insulin resistance (*2*, *10*, *11*). Human studies have revealed an inverse relationship between muscle $C_{18:0}$ ceramides and insulin sensitivity in obese participants (*11*).

While ceramide-induced dysfunction in classic metabolic tissues such as the liver, skeletal muscle, and adipose tissues has been well defined, there has been an underappreciation for where ceramides are predominantly produced and how they are packaged to circulate the body to influence metabolic tissue function. Evidence suggests that ceramides are released from the liver within low-density lipoproteins (LDLs) and contribute to skeletal muscle insulin resistance and pro-inflammatory responses in macrophages (*8*). It has, therefore, been assumed that most of the systemic ceramide pools are supplied by the liver, although organs such as the gastrointestinal tract have also been implicated in this process (*12*).

Following the consumption of fatty foods, lipid digestion begins in the oral cavity then continues in the stomach aided by lipase enzymes. This digestion combined with mechanical mixing leads to the formation of a crude emulsion within the stomach that progresses to the duodenum. Further digestion, here, by pancreatic lipase enzymes and biliary components such as bile salts results in the formation of lipid vesicles and micelles from which lipid digestion products are absorbed across the intestinal wall (*13*).

Dietary sphingolipid consumption in a typical Western diet provides <0.02% of caloric intake, equating to ~0.4 g of sphingolipids consumed daily, most of which is sphingomyelin (*14*). Now, the nutritional requirements and the function of dietary ceramides are not well established; however, it is known that dietary sphingolipids undergo hydrolysis and absorption by the intestinal epithelium (*15*). Furthermore, early studies have demonstrated that small amounts of radiolabeled sphingolipid base can be found in the liver, systemic blood, and lymph of rats fed sphingoid base–labeled sphingolipids

[1]Monash Institute of Pharmaceutical Sciences, Monash University, Melbourne, Australia. [2]Surgical and Translational Research Centre, Faculty of Medical and Health Sciences, The University of Auckland, Auckland, New Zealand. [3]HBP/Upper GI Unit, Department of General Surgery, Auckland City Hospital, Auckland, New Zealand. [4]Max Planck Institute for Metabolism and Cologne Excellence Cluster on Cellular Stress Responses in Aging Associated Diseases (CECAD), Cologne, Germany. [5]University of Cologne, Faculty of Medicine and University Hospital of Cologne, Cluster of Excellence Cellular Stress Responses in Aging associated Diseases (CECAD), Cologne, Germany. [6]Biomedical Discovery Institute, Monash University, Melbourne, Australia. [7]Applied Surgery and Metabolism Laboratory, School of Biological Sciences, The University of Auckland, Auckland, New Zealand.
*Corresponding author. Email: Sarah.Turpin-Nolan@monash.edu (S.M.T.-N.); Mark.Febbraio@monash.edu (M.A.F.)

(*16*, *17*), thus highlighting that consumed lipids are digested and transported systemically via the lymphatic and circulatory transport systems.

Enteral sphingolipid metabolism is gaining recognition as an important regulator of intestinal nutrient uptake and gut communication within the body during metabolic disease (*7*). Specifically, sphingolipids in the gut lumen can regulate intestinal barrier integrity, and bacterially derived sphingolipids can modulate systemic metabolism by manipulating host hepatic sphingolipid synthesis (*18*). The importance of intestinal-specific generation and export of the metabolically toxic sphingolipid ceramide is becoming increasingly appreciated. A recent study by Li *et al.* (*19*) deleted the rate-limiting enzyme serine palmitoyl transferase 1 or 2 (Sptlc1 or Sptlc2) of the de novo sphingolipid pathway in the intestinal epithelium, which significantly reduced intestinal saturated ceramide species, $C_{16:0}$-$C_{24:0}$, demonstrating that the intestinal epithelial cells (IECs) can generate ceramides. Furthermore, high-fat feeding was able to selectively increase these ceramide species in only the small intestinal regions, not the colon (*19*), suggesting that ceramide production in key small intestinal regions of lipid absorption could be important for intestinal lipid metabolism, chylomicron assembly, and delivery to peripheral tissues. An association between intestinal tissue ceramide content and systemic serum ceramide concentrations has been observed and was thought to be modulated via the intestinal farnesoid X receptor's (FXR) inhibition of genes involved in ceramide synthesis (*12*). These previous studies assume, however, that ceramides are being directly exported from the intestine into the bloodstream, which appears unlikely given that other lipid species such as dietary triacylglycerols (TAGs), phospholipids, and cholesterols are assembled into intestinal chylomicrons, which are transported via the mesenteric lymphatics before emptying into the bloodstream (*20*).

Here, we aimed to evaluate the mechanisms of intestinal generation, assembly, and export of ceramides, including the role of chylomicrons and the lymphatic transport system. Our results have identified a unique lipidomic signature in mesenteric lymph-derived chylomicrons marked by previously undisclosed lipid species from the sphingolipid and glycerophospholipid lipid families. Furthermore, consumption of a high-fat diet (HFD) has a profound effect on the lipid composition in chylomicrons, of which the abundance of metabolically toxic ceramide species is elevated in both rodents fed an HFD and humans receiving a nutritional lipid overload.

## RESULTS

### $C_{16:0}$ ceramides are highly abundant in plasma and the intestinal epithelium and increase in mice fed an HFD

To identify if circulating levels of different ceramide species are responsive to feeding, we performed a comparison of circulating ceramides, captured during the fed state, in both chow and HFD-fed mice. Acyl chain–specific differences were observed in mice that were refed following an overnight fast with $C_{16:0}$, $C_{22:0}$, and $C_{24:0}$, the most predominant systemic circulating ceramides irrespective of diet consumption (Fig. 1A). Furthermore, the consumption of an HFD to increase fatty acid (FA) availability and drive de novo ceramide production resulted in elevations of shorter and medium chain length $C_{16:0}$, $C_{18:0}$, $C_{20:0}$, and $C_{22:0}$ ceramides with the greatest increase observed for $C_{22:0}$ ceramides (Fig. 1A).

Although sphingolipids are abundant throughout the gastrointestinal tract (*18*, *21*), an acyl chain–specific analysis of sphingolipid synthesis and export from the intestinal epithelium through the lymphatics system is yet to be defined. To determine sphingolipid levels and their relative abundance in key tissues and compartments along the intestinal-lymphatic axis, a targeted lipidomic screen was performed by liquid chromatography–mass spectrometry (LC-MS) in isolated IECs to quantify ceramide and sphingomyelin concentrations. In the duodenal and jejunal regions, which are identified to be the predominant lipid absorbing regions of the small intestine, all saturated ceramide species were increased with high-fat feeding (Fig. 1, B and C). $C_{16:0}$ ceramides were the most abundant across diet groups and were markedly elevated in HFD-fed animals compared with control mice (Fig. 1, B to D). In the ileum, however, the effect of HFD-induced $C_{16:0}$ ceramide production, ~34% increase (Fig. 1D), was much less pronounced compared to a ~65% increase in the duodenum and jejunum regions (Fig. 1, B and C). Last, colonic ceramide levels were slightly elevated with HFD feeding, but only $C_{18:0}$ and $C_{20:0}$ ceramides were increased with HFD (Fig. 1E). While the shorter-chain $C_{16:0}$ ceramides were still the most abundant in the colon, it appears that the increase in ceramide species accumulation in response to HFD-feeding is more apparent in the regions of the small intestine typically involved with nutrient uptake and lipid absorption. Together with the study by Li *et al.* (*19*), these data demonstrate that intestinal cells involved in nutrient uptake are able to generate ceramides. Moreover, overconsumption of lipid substrates in our diet appears to drive ceramide production and accumulation within the intestinal epithelium.

### Intestinal ceramide profiles do not directly correlate with ceramide profiles of the liver and blood

We next sought to determine whether the HFD-induced increase in ceramide accumulation reported above was directly attributable to ceramide accrual within the IECs. As the previous results were conducted in two independent laboratories (refer to Materials and Methods for details), the aim of this second study was to determine whether the newly synthesized intestinal ceramides were transported within lymph or blood. To do this, we used the lymph cannulated Sprague-Dawley rat model for ease of surgical cannulation success and to enable a cross-species comparison between mice and rats. Lipidomic screening in rat IECs revealed the short-chain ceramide abundance was enriched in the duodenal and jejunal of the small intestine but not the ileum, consistent with the results reported in our HFD mice (Fig. 2, A to C). Furthermore, high-fat feeding only elevated $C_{16:0}$ and $C_{18:0}$ ceramides in duodenal epithelial cells, while only $C_{14:0}$ ceramide accumulation was increased in the jejunum of the HFD-fed rats compared with chow-fed controls (Fig. 2, A and B). Ileal ceramides, by contrast, were unaffected by HFD-feeding in rats (Fig. 2C). To confirm that the HFD was increasing the de novo flux of ceramide synthesis, we found that, indeed, the more highly abundant shorter-chain sphingomyelin species downstream of ceramide synthesis were markedly increased, and $C_{16:0}$ sphingomyelin was the most abundant sphingomyelin species in both duodenal and jejunal regions (Fig. 2, D to F). Together, these data suggest that $C_{16:0}$ sphingolipid species are the most predominant in the small intestinal regions, but relative abundance was highest in duodenum > jejunum > ileum (Fig. 2), consistent with expected $C_{16:0}$ FA availability from the diet.

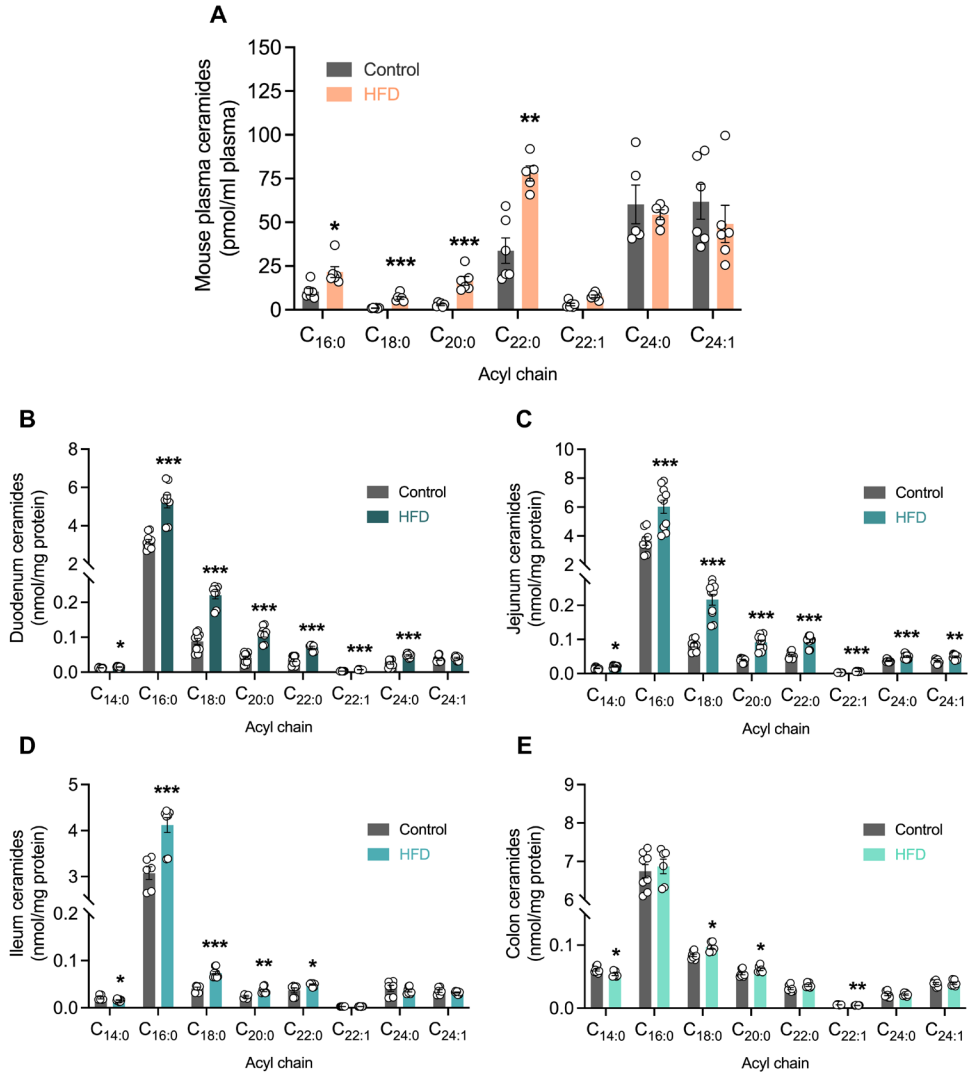


**Fig. 1. Ceramides increase in the circulation and gut epithelium in response to high fat feeding.** (**A**) Lipidomic quantitation of individual ceramide species in plasma samples obtained after refeed from mice fed either a control or high-fat diet (HFD). $n = 6$. Lipidomic quantitation of individual ceramide species in isolated gut epithelial cells from the (**B**) duodenal, (**C**) jejunal, (**D**) ileal, and (**E**) colonic regions of mice fed a control or HFD. (B and C) $n = 8$ to 10 and (D and E) $n = 6$ to 8. Data are expressed as means ± SEM. *$P < 0.05$, **$P < 0.01$, and ***$P < 0.001$.

To determine whether intestinal generated ceramides were directly entering the circulatory system for delivery to metabolic organs, we collected blood from the superior mesenteric vein (intestine-derived) and the heart (systemic representative) and compared the serum ceramide profiles (Fig. 3, A and B). Unexpectedly, the ceramide profiles were very similar, and there was no increase in circulating ceramides levels during feeding in HFD-fed rats compared with controls. Further evaluation of both the intestinal and systemic ceramide profiles showed that these serum profiles did not match those of the small IEC regions. Specifically, the most abundant ceramide species in the serum were the $C_{22:0}$ and $C_{24:0}$ ceramides (Fig. 3, A and B), while in the intestinal epithelium, it was $C_{16:0}$ ceramides (Fig. 2, A and B). To confirm that the cannulation surgery did not alter the ability of the small intestine to synthesize ceramides and release them into the circulation, a second cohort of sham rats underwent an identical dietary intervention and anesthetic procedure as the previously cannulated rats (fig. S1, A and B). Once the sham rats were anesthetized, serum and intestinal tissues were removed and analyzed, demonstrating that the intestinal ceramide profiles mirrored the cannulated rat results to confirm that intestinal ceramides do not appear to directly enter the circulatory system (fig. S1A). Furthermore, the cardiac serum confirmed that the removal of lymph during the cannulation collection procedure did not affect the ceramide species present in the serum (fig. S1C). This then raised the question if the serum ceramide profiles did not match those of the small intestinal regions, then would they match those of the liver, another major tissue known to generate and export ceramides around the body?

The comparison of the hepatic tissue ceramide profiles from the cannulated rats revealed that the expression pattern of hepatic ceramides showed a greater abundance of longer-chain $C_{22:0}$-$C_{24:0}$ ceramide species (Fig. 3C). While the hepatic tissue levels of $C_{24:0}$ and $C_{22:0}$ ceramide species were not affected by high-fat feeding, the

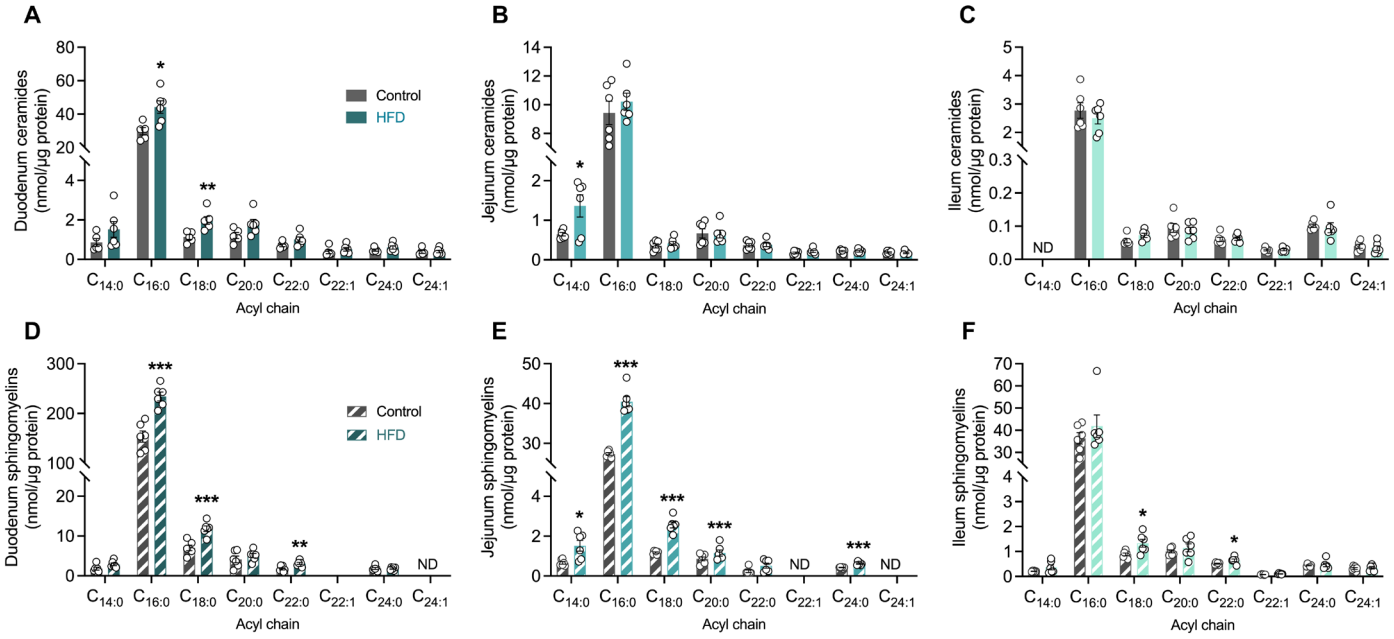


**Fig. 2. Shorter-chain sphingolipids are highly abundant in the rat small intestine and selectively increase in response to high-fat feeding.** Lipidomic quantitation of individual ceramides (solid bars) in (**A**) duodenal, (**B**) jejunal, and **(C**) ileal epithelial cells, and sphingomyelins (striped bars) in (**D**) duodenal (**E**) jejunal, and (**F**) ileal epithelial cells from in rats fed either a control or an HFD. The number of biological replicates $n = 5$ to 6 per diet group in each experiment. Data are expressed as means ± SEM. $^{*}P < 0.05$, $^{**}P < 0.01$, and $^{***}P < 0.001$.

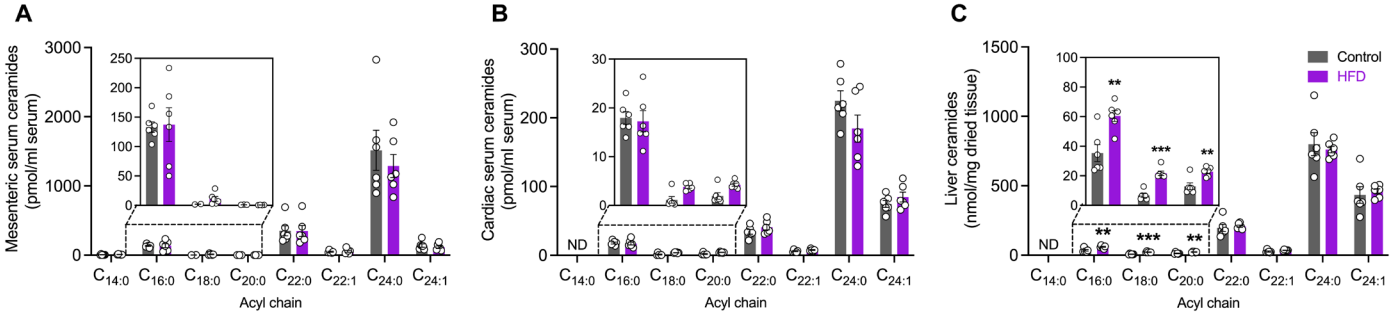


**Fig. 3. Circulating ceramide profiles are more reflective of the liver, not the intestine.** Lipidomic quantitation of individual ceramides (solid bars) in (**A**) super mesenteric serum and (**B**) cardiac serum or the (**C**) liver of rats fed either a control or an HFD. The following numbers of biological replicates were used (independent rats) per diet group in each experiment: (A to C) $n = 6$. Data are expressed as means ± SEM. $^{**}P < 0.01$ and $^{***}P < 0.001$.

relative abundance of $C_{24:0}$ and $C_{22:0}$ ceramides were noticeably greater than $C_{16:0}$ ceramides irrespective of diet. Likewise, ceramide profiles in both the systemic circulation and in serum sampled from the superior mesenteric vein were near identical to the liver tissue, but not the duodenum or jejunum, in terms of relative abundance and dietary effect (Fig. 3, A to C). This suggests that the hepatic ceramide profile was more reflective of the circulating ceramide profiles and that ceramides in the circulation are more likely to be derived, mostly, from the liver rather than the intestine when animals are in the fed state.

## Chylomicrons contain distinct lipidomic signatures, but not all lipid species increase upon HFD consumption

Lipid digestion and uptake from dietary sources begins in the intestinal lumen where nutrients are digested and absorbed into intestinal enterocytes, re-esterified, and assembled into chylomicrons with the specific apolipoprotein B48 and then released into the lymphatic transport system. Now, it is recognized that chylomicrons contain TAGs, cholesterol esters, cholesterol, phospholipids, and apolipoproteins (*22*, *23*), but whether other lipid species can be transported in chylomicrons or if all lipid species uniformly increase upon high-fat consumption is unclear. Lymph from the small intestine originates from lymphatic capillaries (lacteals) embedded within individual intestinal villi; these lacteals converge at the mesenteric collecting lymph ducts before reaching the centrally located thoracic duct (*20*). To accurately quantify lipids exported from the small intestine, the efferent superior mesenteric lymph duct was cannulated in control and HFD-fed rats. Lymph was collected and analyzed to determine whether ceramide species were, indeed, exported into the lymphatics, and whether the ceramide profiles were reflective of the IEC ceramide production.

Lipidomic analysis revealed that ceramides were present in intestinal-derived lymph and that $C_{16:0}$ ceramides were the most abundant ceramide species regardless of diet, consistent with the previously detected ceramide species in the rat small intestines (Fig. 4A). High-fat feeding elevated $C_{14:0}$, $C_{16:0}$, $C_{22:0}$, and $C_{22:1}$ ceramide species in mesenteric lymph, with the greatest increase observed for $C_{16:0}$ ceramides (Fig. 4A). This increase was reflective of amplified $C_{16:0}$ FA processing as multiple lipids with incorporated $C_{16}$ carbon FA chains were elevated in chylomicrons isolated from mesenteric lymph (fig. S2). Sphingomyelin levels in mesenteric lymph were also reflective of this paradigm, wherein $C_{16:0}$ sphingomyelin was the most abundant subspecies, although not significantly elevated in obese animals (Fig. 4B).

Lymphatic delivery of intestinal-derived lipids is facilitated by chylomicrons, the predominant intestinal lipoprotein carrier. The hydrophobic core of a chylomicron not only consists mainly of TAGs and cholesterol esters but—similar to other lipoprotein classes, proteins, and other lipid species such as cholesterols and phospholipids—is also incorporated into the chylomicron surface to increase stability, albeit at much lower concentrations (*24*). While the existence of total ceramides has previously been reported in chylomicrons isolated from the thoracic lymph duct (*25*, *26*), little is known of individual sphingolipid levels incorporated into intestinal-derived chylomicrons and how they vary with dietary intervention. To further probe the intestinal-derived chylomicron lipidome, the chylomicron lipoprotein fraction was isolated from mesenteric lymph and underwent lipidomic analysis to not only quantify ceramide species but also identify other lipid classes that may increase upon the consumption of an HFD. Short-chain $C_{16:0}$ ceramides were, importantly, the most abundant ceramide subspecies in the chylomicron fraction and were increased 1.7-fold, with high-fat feeding (Fig. 4C). In addition, $C_{14:0}$ ceramides were also elevated in obese animals, which possibly reflects the up-regulation of the specific ceramide synthase enzymes, ceramide synthase 5 and 6, the two enzymes responsible for the synthesis of $C_{14:0}$ and $C_{16:0}$ ceramides. Sphingomyelin levels, although not significantly altered with diet, were also detected within the chylomicron lipidome with $C_{16:0}$ sphingomyelin demonstrating the highest concentration relative to other detected sphingomyelin species but unexpectedly did not increase in response to high-fat feeding (Fig. 4D). In addition to the sphingolipid profiles, FAs, diacylglycerols (DAGs), and TAG species containing a $C_{16}$ carbon FA chain were also significantly increased with HFD (fig. S2). Various other glycerophospholipid species with a $C_{16}$ carbon FA chain, such as phosphocholines (PCs) and phosphoethanolamines (PEs), were unaffected by increased $C_{16:0}$ FA substrate availability (fig. S2).

To unveil the full spectrum of lipid diversity within the chylomicron core, an untargeted quantitation of lipids was performed on isolated chylomicrons from both control and HFD-fed animals. Furthermore, key lipid classes detected within the chylomicron, in addition to ceramides and sphingomyelins, included phosphates,

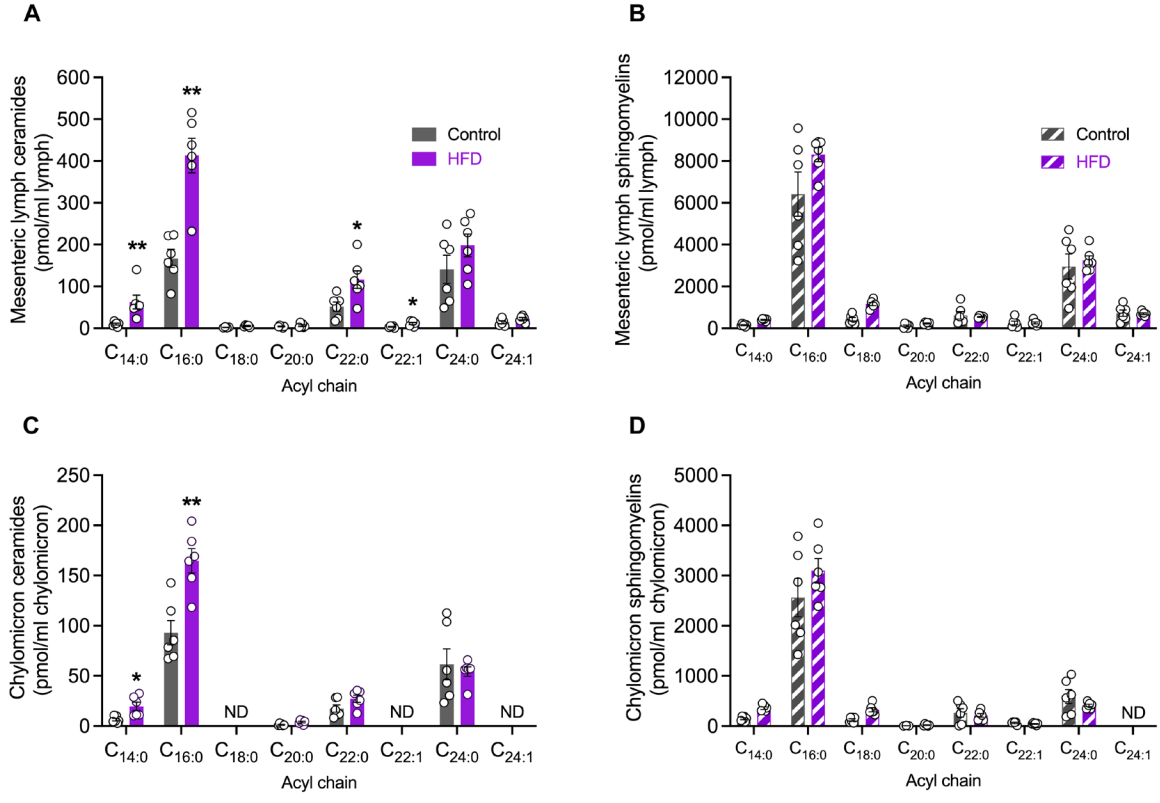


**Fig. 4. High-fat feeding fuels ceramide, but not sphingomyelin, accumulation in mesenteric lymph-derived chylomicrons.** Lipidomic quantitation of (**A**) individual ceramides (solid bars) or (**B**) sphingomyelins (striped bars) in mesenteric lymph of rats fed either a control or an HFD. Lipidomic quantitation of (**C**) individual ceramides or (**D**) sphingomyelins in chylomicrons isolated from the mesenteric lymph of rats fed either a control or an HFD. The following numbers of biological replicates were used (independent rats) per diet group in each experiment: (A to D) $n = 6$. Data are expressed as means ± SEM. $^*P < 0.05$ and $^{**}P < 0.01$.

PC, PE, phosphoglycerols (PGs), phosphoinositols (PIs), and phosphoserines (PSs) (Fig. 5). The heatmap generation of individual lipid analytes from each lipid class revealed that key alterations in the chylomicron lipidome with high-fat feeding was not uniform across lipid classes, with the most up-regulated changes evident in saturated PC and PE acyl lipids and PE in the ether lipid classes (Fig. 5, signified by color change from yellow to red, and figs. S3 to S5). It was interesting to note that the PC, PE, and PI acyl lipid families contained the most quantifiable lipid analytes of any lipid analyte family (Fig. 5 and figs. S3 to S5). The detectable PS acyl lipids were all down-regulated (signified by color change from yellow to green/blue) in the HFD chylomicrons, highlighting that the availability of saturated FA substrates to enterocytes does not always drive the synthesis of all lipid species (Fig. 5 and figs. S3 to S5). Together, these results demonstrate that the intestinal production and export of distinct lipid species is highly specialized, once again highlighting the potential importance of changes to intestinal-derived $C_{16:0}$ ceramide abundance in response to lipid consumption and metabolic tissue dysregulation.

### Enteral feeding of a lipid emulsion solution increases $C_{16:0}$ ceramides in human lymph

Because we identified that ceramides are incorporated into chylomicrons in the intestine and that $C_{16:0}$ ceramides increase in response to an HFD in rodents (Fig. 4), we next sought to determine whether these observations were relevant to humans. Thoracic lymph fluid was collected via insertion of a cannula into the thoracic lymph duct during an Ivor Lewis oesophagogastrostomy procedure (*27*). Thoracic lymph, rather than mesenteric, was collected as the mesenteric lymphatics are deep within the abdomen, and a more invasive surgery would be required. Nonetheless, the lipids in thoracic lymph are largely derived from the intestine as previous studies have shown that ~50% of thoracic lymph fluid originates from the intestine (*28*).

Specifically, the patient underwent an Ivor Lewis oesophagogastrectomy in which they required an enteral feeding tube inserted in the proximal jejunum, and a Nutrison standard enteral feeding solution that contained 16% energy from protein, 49% energy from carbohydrates, and 35% energy from fat was infused at differing flow rates. Over time, the rate of enteral lipid infusion increased, which resulted in more lipids being presented to the small intestinal lumen and, thus, more lipids available for absorption. Thoracic lymph samples were able to be regularly collected proximal to the oesophagogastrectomy site. While these lymph samples were not directly determining the ceramide content in human mesenteric lymph, previous studies, including by our group (*28*), have shown that at least ~50% of the lymph entering the thoracic duct is composed of mesenteric lymph. This, therefore, enabled an indirect measurement of intestinal-assembled ceramides in human lymph and determine whether thoracic lymph ceramides changed in response to the increasing amount of enteral lipid meal replacement solution delivered to the lumen of the small intestine.

The quantification of the lipid content in the thoracic lymph had previously demonstrated that increasing enteral feeding concurrently promoted TAG transport in response to increased flow rates (*29*). This observation was reconfirmed with metabolomic quantitation (tables S1 and S2). The data demonstrated that only the TAGs, and not DAGs, moderately increased in the thoracic lymph when the patient was receiving post-enteral feeding of Nutrison at a rate of 20 ml/hour compared to the baseline of 0 ml/hour (Fig. 6A). In the same patient, however, when the post-enteral feeding rate of Nutrison was increased to 80 ml/hour, TAGs and DAGs increased by 153 and 113%, respectively (Fig. 6B). These data strongly suggested that enteral lipid feeding was increasing the production and assembly of intestinal-derived chylomicrons due to the increased levels of TAG and DAGs in the patient's thoracic lymph.

To determine whether human lymph also contained ceramides, samples collected from the oesophagogastrectomy patient's thoracic lymph duct at two different time points after surgery were evaluated (fig. S6, A and B, and tables S1 and S2). While both ceramide profiles were similar between D0 (fig. S6A) and D1A1 (fig. S6B), the latter was chosen as the baseline control to eliminate any potential bias from the intestinal milk cream bolus (high sphingolipid content) that was administered before the D0 time point to aid in lymphatic duct visualization by surgeons. It was confirmed that human lymph contained ceramides, and $C_{24:0}$ ceramide was the most predominant species (tables S1 and S2). This was different to our control diet-fed rats (Fig. 4), which showed that both $C_{16:0}$ and $C_{24:0}$ were the most predominant ceramide species (Fig. 4, A and C).

We then sought to confirm that human ceramide profile in circulating lymph changed in response to increased lipid load in the small intestine. The comparison of baseline to a post-enteral feeding rate of Nutrison of 20 ml/hour found that of all detectable ceramide species, the lowest detectable ceramide specie, $C_{16:0}$ ceramide, showed the greatest, sixfold, increase in thoracic lymph (Fig. 6E). Further studies increasing the enteral lipid flow rate of Nutrison to 80 ml/hour (Fig. 6F) again showed that $C_{16:0}$ ceramide species was the most elevated of all the ceramides as it increased 26-fold from the baseline, 20-fold higher than when the patient was receiving the Nutrison infusion (20 ml/hour) (Fig. 6, E and F). The extent to which $C_{16:0}$ ceramide species elevated in response to human enteral feeding was not expected and demonstrates that the transport of $C_{16:0}$ ceramides from the gut via the lymphatics is important and highly complex. This finding further underscores the importance of circulating dietary-derived $C_{16:0}$ ceramides and their delivery from chylomicrons to metabolic tissues.

Together, this human study highlights that ceramides are produced and packaged in the small intestine in response to lipid availability in the diet. Furthermore, the measurement of plasma ceramide levels more accurately reflects the ceramide profile of the liver rather than the nutritional state following the consumption of a high lipid meal. These results have identified a unique transport axis for ceramides, provided insight into how lipids are digested and transported throughout the body in response to a fatty meal, and highlighted a new paradigm for therapeutic strategies trying to lower $C_{16:0}$ ceramide accumulation in peripheral metabolic tissues.

## DISCUSSION

Ceramides have long been associated with metabolic diseases, and the liver has been understood to be the primary site of ceramide production and the main contributor to the production and transfer of metabolically deleterious ceramides to other organs (*30*–*32*). What is underappreciated, however, is that ceramide accumulation is associated with a diet rich in saturated fats and that dietary fats are first metabolized in the intestine. Here, we identified a unique sphingolipid expression pattern in the intestinal tract that was profoundly different to the liver and altered in obesity, resulting in the accumulation of metabolically pathogenic $C_{16:0}$ ceramides in intestinal-derived chylomicrons (Fig. 4C).

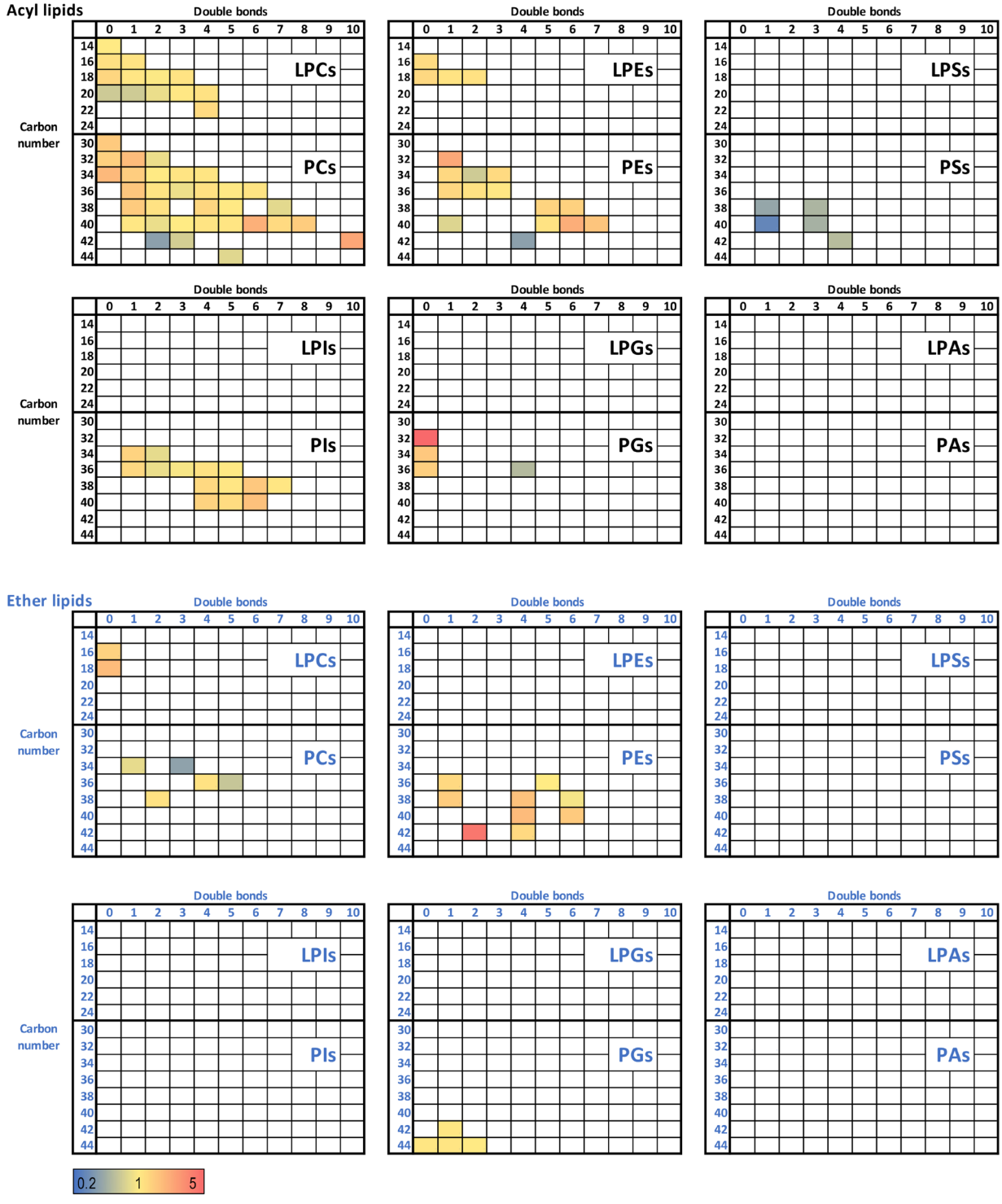


**Fig. 5. High-fat feeding induces a shift in the proportion of lipid classes in lymph-derived chylomicrons.** Untargeted lipidomic analysis of individual acyl lipids and ether lipids sorted by class (facets), double bond (*x* axis) and carbon atom number (*y* axis) in isolated mesenteric lymph-derived chylomicrons. Data were expressed as fold change HFD/control. Color coding: yellow, no change; red, up-regulated in HFD; blue, down-regulated in HFD; white, not detectable. PEs, phosphoethanolamines; PAs, phosphatidic acids; PGs, phosphoglycerols; PIs, phosphoinositols; PSs, phosphoserines; PCs, phosphocholines; LPCs, lysophosphatidylcholines; LPEs, lysophosphatidylethanolamines; LPAs, lysophosphatidic acids; LPGs, lysophosphatidylglycerols; LPSs, lysophosphatidylserines; LPIs, lysophosphatidylinositols.

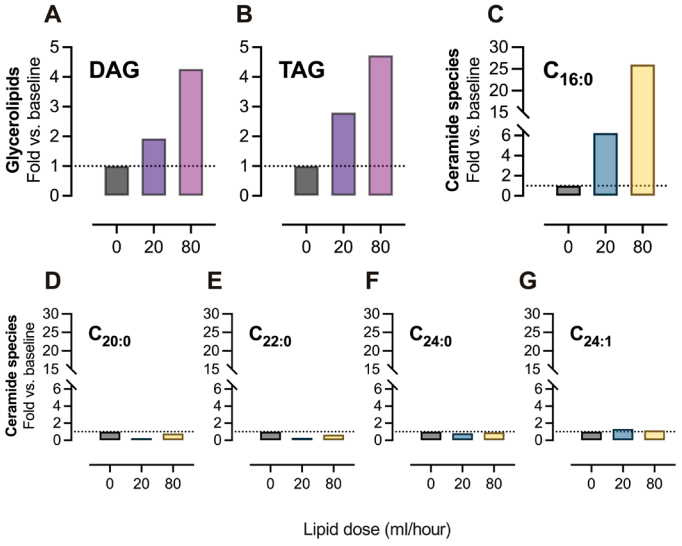


**Fig. 6. Human enteral feeding of a lipid meal replacement selectively increases $C_{16:0}$ ceramides in thoracic lymph.** Human thoracic lymph sampling was performed before and during Nutrison enteral feeding of a patient after undergoing an Ivor Lewis oesophogastrectomy. Fold change from baseline (enteral feed, 0 ml/hour) of (**A**) DAG and (**B**) TAG levels in thoracic lymph from the patient undergoing enteral lipid feeding of 20 and 80 ml/hour. Fold change from baseline of (**C**) $C_{16:0}$, (**D**) $C_{20:0}$, (**E**) $C_{22:0}$, (**F**) $C_{24:0}$, and (**G**) $C_{24:1}$ individual ceramide species in thoracic lymph from a patient undergoing enteral lipid feeding of 20 and 80 ml/hour. DAG, diacylglycerol; TAG, triacylglycerol.

The effect of dietary manipulation on ceramide abundance has been well characterized in key organs associated with metabolic disease such as the liver (*9*), skeletal muscle (*2*), white adipose tissue (*1*), and brain (*33*, *34*). High-fat feeding has consistently been shown to increase circulating ceramide levels in mice (*35*–*38*) and obese human patients (*8*, *39*), and these ceramide species are currently being used as biomarkers to predict metabolic and cardiovascular events (*40*–*42*). However, the dietary influence on gut-produced ceramides is not well characterized. Recently, evidence has emerged, suggesting that intestinal ceramide synthesis is an important regulator of barrier function (*19*, *43*, *44*). The deletion of key enzymes *Sptlc1*, *Sptlc2*, or *CerS2* has been found to regulate the production of ceramides through the de novo sphingolipid pathway to significantly reduce complete (*Sptlc1* or *Sptlc2*) or selective (*CerS2*) ceramide levels throughout the small intestine (*19*, *43*, *44*). Furthermore, Li *et al.* (*19*) found the consumption of an obesogenic HFD with lard as the primary fat source increased levels of ceramides ($C_{16:0}$, $C_{18:0}$, and $C_{24:0}$) in jejunal crypts but not villi, and $C_{16:0}$ ceramides were the most predominant species.

While there are a series of studies from Gonzalez's laboratory detailing ceramide levels in murine ileal tissue (*12*, *45*), these studies focused on the regulatory capacity of intestinal FXR in nonalcoholic fatty liver disease progression rather than dietary lipid intervention. These findings are suggestive of, both, a dietary regulated effect upon intestinal ceramide synthesis and described ceramide transit from the gut into the circulation (*12*, *45*). While a direct link between the gut and circulating levels of ceramides was suggested (*12*, *45*), we have demonstrated that ceramides in the circulation are not representative of dietary or intestinal-derived ceramides, and furthermore, ceramides are packaged and exported from the IECs by a completely different mechanism.

The distribution of sphingolipids in common foods and diets varies but is found in abundance in animal and dairy products (*14*, *46*). The consumption of fatty foods greatly enriches the gastrointestinal lumen with various sphingolipid species, and the microbiome also contributes to sphingolipid abundance and diversity (*18*). Recent findings have shown that complex sphingolipids found in everyday foods have little impact on intestinal sphingolipid accumulation as they are poorly absorbed by the intestine and are instead preferentially metabolized into FAs (*15*). This suggests that the intracellular production of ceramides detected within enterocytes is driven by the availability of lipid substrates, such as palmitate, as opposed to the direct transport of ceramide and other sphingolipids into enterocytes. We therefore used HFD feeding [containing 10% saturated fats (palmitic acid and stearic acid), 8% monounsaturated (oleic acid), and 5% polyunsaturated fats (linoleic acid)] as a tool to provide the necessary substrates to stimulate de novo ceramide synthesis in the intestinal epithelium. Furthermore, a diet rich in $C_{16:0}$ FAs (palmitic acid) resulted in the generation of multiple lipids from different lipid classes containing a $C_{16}$ FA carbon chain, including $C_{16:0}$ ceramides in the gut and mesenteric lymph, highlighting that $C_{16:0}$ substrate availability can regulate the flux of multiple lipid pathways.

While numerous studies have reported the existence of a rich sphingolipid diversity in the gut tissue (*12*, *18*, *45*), our data are consistent with previous reports of lipidomic analyses for ceramides in ileal tissue from HFD-fed mice (*12*, *45*). From other non-diet–focused studies, ileal $C_{16:0}$ ceramides and sphingomyelins are highly abundant compared to other subspecies, which are detected at trace amounts in animals (*18*) and humans (*47*). This agrees with both the mouse and rat ileum epithelial cell ceramide concentrations, where we found that the epithelial cells lining the rat small intestine have a strong preference for synthesizing shorter-chain $C_{16:0}$ ceramide species (Fig. 2). While high-fat feeding had a minimal effect on ceramide accumulation in all three regions of the obese rat small intestine, it did profoundly elevate metabolically toxic $C_{16:0}$ ceramides in intestinal-derived mesenteric lymph (Fig. 4A). Unlike mice, where hepatic ceramides have been reported to be elevated while on an HFD (*1*, *48*, *49*), the effect of high-fat feeding on ceramide accumulation in the rat liver appeared to be negligible. One suggestion is that rats could be more resistant than mice to dietary stimuli and associated ceramide synthesis in the liver; however, this does not align with existing reports of elevated total ceramide in rat livers after similar HFD regimens, albeit with diets containing a significantly greater lipid composition (*30*, *32*). It has also been suggested that the liver is highly sensitive to intracellular ceramide levels and offsets a toxic accumulation by increasing ceramide efflux into the circulation (*31*). However, one would expect a consequential rise in plasma ceramides, which was not observed in our rat study. Nevertheless, we demonstrated a clear acyl chain preference for the synthesis of longer chain ceramides in the liver as hepatic $C_{16:0}$ ceramide levels were low in the rats. The relative distribution of individual ceramide species in the liver, mesenteric, and cardiac blood, when compared to ceramides along the gut-lymph tract, demonstrated a clear profile disparity, signifying a bona fide intestinal-lymphatic axis for intestinal ceramide export.

The existence of ceramides in thoracic lymph and associated chylomicrons is evidenced dating back 40 years (*25*, *26*, *50*); however, these studies use crude determinations of lipid composition measuring total

sphingolipids or ceramide content. More recent investigations have determined that ceramides species are present in the thoracic lymph (*51*–*54*), which in turn consists of ~50% derived from the intestine, but no study has directly determined the production and assembly of ceramides into chylomicrons before lymphatic endothelial lipoprotein lipase can hydrolyze and release chylomicron lipids within the lymphatic vessel walls (*20*). Our study directly assesses the profiles of intestinal ceramide species and compares this profile, with that directly released into the intestinal lymphatic ducts.

Chylomicrons are produced by IECs in response to intestinal lipid availability (*55*, *56*) and contain a fatty lipid core consisting of TAGs, diglycerides, cholesterol esters, and the surface lipids, which are cholesterols, apolipoprotein B48, and phospholipids that act as surfactants (*22*, *23*, *57*). Recent publications by Cao *et al.* (*58*) describe a rich lipid diversity within isolated intestinal-derived lymph in HFD-fed mice, while Hong *et al.* (*59*) further isolated lymph-derived TAG-rich lipoproteins and categorized the detected lipid families in sepsis and gut ischemia-reperfusion injury rat models. We found a similar distribution of lipids in intestinal-derived chylomicrons, albeit with slight discrepancies in the total number of identified analytes, which are most likely due to the differences in feed composition, as ours contained a significantly higher fat content to promote lipid synthesis and flux through the intestinal-lymphatic system. Our results identified more chylomicron lipid species than the previous studies and, more importantly, identified individual lipid species that increased upon the consumption of an HFD (figs. S3 to S5). Furthermore, we report that chylomicrons are greatly enriched in $C_{16:0}$ ceramide species, which matches the lipidomic profile of the small intestine, where $C_{16:0}$ ceramides were the most abundant species (Fig. 2, A to C).

The lack of studies detailing the lipid composition of human mesenteric or thoracic lymph and derived chylomicrons reflects the extreme difficulties in acquiring these lymph samples from patients. Traditional methods to access lymph ducts or vessels have been highly invasive and represent a major obstacle to the collection and investigative studies of lymph composition. Because of this, our understanding of lipid profiles in intestinal derived chylomicrons has come from animal studies (*29*, *51*–*54*, *58*). We report that thoracic lymph from a human patient undergoing a lipid-based feeding regimen (containing double the monounsaturated lipid content compared to both the saturated and polyunsaturated lipid content) increased $C_{16:0}$ ceramide species in response to increased lipid in the small intestinal lumen, demonstrating that $C_{16:0}$ ceramides are produced and packaged in the small intestine in response to dietary lipid availability. Whether this is directly driven by $C_{16:0}$-saturated FA availability remains unknown; however, this is one of the first studies to demonstrate a clear ceramide response to diet mediated through the production of intestinal-derived lymph (containing chylomicrons) that can be translated from small rodents to humans. Together, these results demonstrate the importance of dietary-derived sphingolipid production in enterocytes and highlight that intestinal $C_{16:0}$ ceramide production and delivery in chylomicrons could contribute to metabolic disease. Our results highlight the significance of enterocytes during metabolic diseases as they regulate not only chylomicron production but, more importantly, the amounts of individual lipid species that are incorporated into each chylomicron.

In conclusion, we propose an updated model (Fig. 7) for how the body generates and transports sphingolipids derived from dietary sources. Our results from animal and human models of high-fat feeding show that dietary lipids fuel de novo ceramide synthesis in the enterocyte resulting in the accumulation of metabolically toxic $C_{16:0}$ ceramides in chylomicrons. Future studies are now required to investigate where chylomicron-containing $C_{16:0}$ ceramides are exported to, and if new therapeutics targeting intestinal ceramide production could reduce lipid accumulation in peripheral metabolic organs, including the liver, to treat metabolic diseases such as obesity and metabolic-associated fatty liver disease.

## MATERIALS AND METHODS

### German animal care

German animal care refers to Fig. 1 (B to E). All animal procedures and euthanasia were reviewed by the animal care committee and approved by local government authorities (Tierschutzkommission acc. §15 TSchG of the Landesamt für Natur, Umwelt, und Verbraucherschutz North Rhine Westphalia) and were in accordance with National Institutes of Health (NIH) guidelines. Male C57BL/6N mice were acquired at 3 weeks of age from Charles River Laboratories and held in a virus-free facility at 22° to 24°C on a 12-hour light/12-hour dark cycle. After 1 week of acclimatization in the animal facility, mice were randomly assigned either an HFD (D12492, 60% kcal from fat; Research diets, New Brunswick, NJ, USA) or a sucrose-matched, low-fat diet (D12450 J, 10% kcal from fat; Research diets, New Brunswick, NJ, USA). Mice were fed ad libitum for 24 weeks before being humanely killed, and IECs were isolated (see below for methodology) (*60*) for the lipidomic quantification of ceramide species. Sphingolipid levels were determined by LC coupled to electrospray ionization tandem MS (LC-ESI-MS/MS). Tissues were homogenized in water using the Precellys 24 Homogenizer (PEQLAB). Lipid extraction and LC-ESI-MS/MS analysis were performed as previously described (*61*). Samples were measured in duplicate.

### Australian animal care

Australian animal care refers to Figs. 1A, 2, 3, and 4. In mouse, all animal experiments were approved and authorized by the Monash Institute of Pharmaceutical Sciences Animal Ethics Committee under project identification number #18594. Animal handling and housing were conducted in accordance with the Monash University Animal Care and Australian National Health and Medical Research Council (NHMRC). C57Bl/6MARP mice (6 weeks old) were housed in groups of four and fed a standard control diet (20% protein, 8.5% lipid, and 3.2% fiber; Barastoc WEHI Mouse Breeder Cubes Irradiated diet, #102119) or an HFD (20.9% protein, 23.5% lipid, and 5.4% crude fiber; SF04-001, Specialty Feeds) with free access to food and water under a standard 12-hour light/12-hour dark cycle. The C57Bl/6MARP mice were fed their respective diets for 8 weeks before being fasted overnight and refed for 2 hours at the commencement of the light cycle. Mice were humanely killed, and blood was collected via cardiac puncture and spun at 2500*g* for 10 min at 4°C.

In rat, all animal experiments were approved and authorized by the Monash Institute of Pharmaceutical Sciences Animal Ethics Committee under project identification number #19717. Animal handling and housing were conducted in accordance with the Monash University Animal Care and Australian National Health and Medical Research Council (NHMRC). Male Sprague-Dawley rats (10 weeks old) were housed in groups of three or four and fed a standard diet (20% protein, 8.5% lipid, and 3.2% fiber; #102119, Barastoc WEHI Mouse Breeder Cubes Irradiated diet) or an HFD (20.9% protein, 23.5% lipid, and 5.4% crude fiber; SF04-001, Specialty Feeds) for 7 to 8 weeks. All

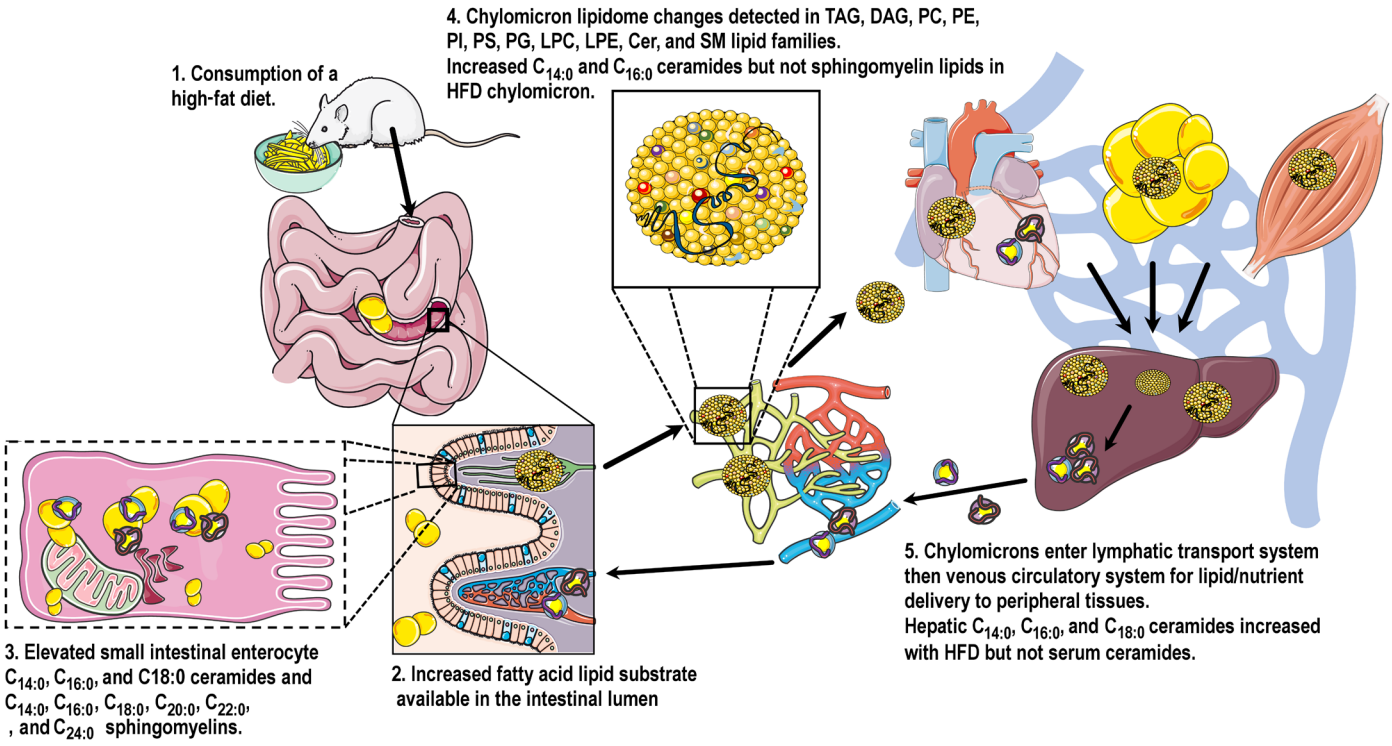


**Fig. 7. Consumption of a high-fat dietary lipid load stimulates enterocyte production of unique lipid species.** A high lipid influx from the diet increases the availability of FA lipid substrate in the lumen of the small intestine. This leads to an elevated accumulation of intracellular ceramides and sphingomyelins in the enterocytes lining the small intestine. Glycerolipid, glycerophospholipid, and sphingolipid lipid families within the chylomicron lipidome are notably altered as a result of increased enterocytic lipid flux, and pathogenic $C_{16:0}$ ceramides are elevated in the obese chylomicron independent of sphingomyelin lipids. $C_{16:0}$ ceramide–rich chylomicrons exit the lymphatics and are circulated around the body via the venous circulation for lipid/nutrient delivery to peripheral tissues.

animals were housed under standard conditions in a 12-hour light/12-hour dark cycle maintained at 22° to 25°C with ad libitum access to food and water.

### Mesenteric lymph collection

The efferent mesenteric lymphatic duct was cannulated in rats as described previously (*62*). Lymph was collected for up to 4 hours in non-fasted animals at the end of the feeding/dark cycle. Briefly, rats were anesthetized by isoflurane inhalation and placed on a heat pad. A midline laparotomy was performed, and layers of connective tissue surrounding the efferent mesenteric lymph duct were removed by blunt dissection. A polyethylene cannula (outer diameter, 0.8 mm; inner diameter, 0.5 mm) prefilled with heparinized saline (10 IU/ml) was passed through the perirenal fat bed, under the kidney, and positioned directly adjacent to the mesenteric lymph duct. The lymph cannula was advanced 1 to 2 mm inside the duct and secured with cyanoacrylate tissue adhesive. Lymph flowed through the cannula and was collected in an Eppendorf tube. Lymph was then centrifuged (300*g*, 5 min, 4°C) to remove endothelial and immune cells before being snap-frozen in liquid nitrogen and stored at −80°C for further analysis. Rats were euthanized, under anesthesia, by exsanguination. Cardiac blood was centrifuged (2500*g*, 10 min, 4°C) to isolate serum, and metabolic tissues were collected, snap-frozen in liquid nitrogen, and stored at −80°C.

### Intestinal epithelial cell isolation

Small intestine regions and the colon were segmented and cleaned in ice-cold phosphate-buffered saline (PBS) as described previously by Ostermann *et al.* (*63*). Mesenteric adipose tissue and Peyer's patches were carefully removed. Intestinal segments were opened longitudinally and vortexed in ice-cold PBS. IECs were separated from the lamina propria by means of digestion for 20 min at 37°C with horizontal rotation in predigestion solution (1× Hanks' balanced salt solution, 10 mM Hepes, 5 mM EDTA, 1 mM dithiothreitol, and 2% fetal bovine serum) followed by vortexing (*60*, *63*). The digestion solution, containing isolated IECs, was passed through a 100-μm cell strainer (BD Bioscience). Digestion was repeated, and supernatants containing isolated IECs were combined. IECs were collected by centrifugation (80*g*, 10 min, 4°C), snap-frozen, and stored at −80°C for further analysis.

### Chylomicron isolation from mesenteric lymph

Lipoprotein fractionation of mesenteric lymph was performed by density gradient ultracentrifugation as previously described (*28*). Plasma background solution was prepared by dissolving 11.42 g of sodium chloride (NaCl) in 1 liter of TE buffer [10 mM tris-HCl and 1 mM disodium EDTA (pH 7.4)]. The density of the background solution was corrected to $\rho = 1.0063$ g/ml by the addition of NaCl or TE buffer. To prepare different density solutions, 1.83, 21.73, or 32.55 g of KBr were dissolved in 100 ml of plasma background solution, and the density was adjusted to 1.02, 1.15, and 1.21 g/ml, respectively, by the addition of KBr or buffer as required. The density of the solutions was confirmed by measuring the refractive index (RI) values of the solution using a refractometer (Mettler Toledo Refracto 30 GS, Mettler Toledo, VIC Australia). RI values were converted to

density values using standard KBr and NaCl salt tables. Density solutions and lymph were layered into 4.2-ml polypropylene centrifuge tubes (Beckman Coulter, CA, USA) in the following order (from bottom to top): 0.31 ml of $\rho = 1.21$ g/ml solution, 1.25 ml of $\rho = 1.15$ g/ml solution, 1 ml of mesenteric lymph, and 1.44 ml of $\rho = 1.02$ g/ml solution. The tubes were placed into the bucket of a SW 60 Ti Rotor (Beckman Coulter) and centrifuged at 453,300*g*, 15°C, for 19 hours (Optima XE-90, Beckman Coulter). After centrifugation, the "milky" chylomicron-rich top layer of the centrifuged sample was transferred to a separate tube and stored at −80°C until metabolite analyses.

### Lipid extraction

Lipid extraction was performed in plasma (20 μl), mesenteric lymph (20 μl), and the lymph chylomicron fraction (10 μl) using the 1-butanol:methanol (1:1 v/v) single-phase extraction method (*64*). For lipidomic analysis of IECs and liver tissue, lipid extractions were performed as previously described with slight modifications (*65*). Briefly, isolated IECs and pulverized liver tissue were homogenized in a chloroform/methanol/water (1:3:1, v/v) solvent mixture containing 5 μM butylated hydroxytoluene and internal standards. Concentrations of internal standards in the final sample were 100 nM for sphingoid bases and 200 nM for ceramide (d18:1/17:0) and sphingomyelin (d18:1/17:0) standards. Samples were vortexed and shaken at 4°C, sonicated in a water bath with ice for 1 hour, and centrifuged. Approximately 200 μl of the supernatant was transferred to new tubes, and the solvent was evaporated under a stream of nitrogen using a Biotage TurboVap LV evaporation system. Dried lipid extracts were reconstituted in 100 μl of a solvent mixture containing 1-butanol/methanol/water (4.5:4.5:1, v/v) and sonicated for 1 hour, keeping the temperature below 25°C, and supernatants were transferred to glass vials for analysis.

### LC-MS analysis

LC-MS data were acquired on a Q-Exactive Orbitrap mass spectrometer (Thermo Fisher Scientific, Waltham, MA, USA) coupled with a high-performance LC system Dionex Ultimate 3000 RS (Thermo Fisher Scientific). Chromatographic separation was performed on a C8 column Ascentis Express (2.7 μm, 2.1 × 100 mm, Supelco, Merck). The mobile phase A was 40% isopropanol, 8 mM ammonium formate, and 2 mM formic acid, and the mobile phase B was 98% isopropanol, 8 mM ammonium formate, and 2 mM formic acid; the needle wash solution was 50% isopropanol. The gradient program started at 0% B and was increased stepwise to 20% B over 1.5 min, to 28% B over 5.5 min, to 35% B over 1 min, to 65% B over 16 min, and to 100% B over 1 min. Wash at 100% B was continued for 2 min before decreasing to 0% B over the next 2 min, followed by equilibration at 0% B for 1 min. The flow rate was 0.2 ml/min, and column compartment temperature was 40°C. The total run time was 30 min with an injection volume of 10 μl. Mass spectrometer operated in full scan mode with positive and negative polarity switching at 70,000 resolution at 200 mass/charge ratio ($m/z$) with a detection range of 140 to 1300 $m/z$. Heated ESI source was set to 3.5 kV voltage for positive mode and 3.5 kV for negative mode, sheath gas was set to 34, aux gas was set to 13, sweep gas was set to 1 arbitrary units, capillary temperature was maintained at 250°C, and the probe heater temperature was maintained at 190°C. The samples were analyzed as a single batch to reduce batch-to-batch variation and randomized to account for LC-MS system drift over time.

### Data processing using IDEOM

The acquired LC-MS data were processed in an untargeted fashion using the open-source software IDEOM (*66*), which initially used ProteoWizard to convert raw LC-MS files to mzXML format and XCMS to pick peaks to convert to peakML files. Mzmatch.R was subsequently used for the alignment of samples, and the filtering of peaks using a minimum detectable intensity of 100,000, relative standard deviation (RSD) of <0.5 (reproducibility), and peak shape (codadw) of >0.8. Mzmatch was also used to retrieve missing peaks and annotation of related peaks. Default IDEOM parameters were used to eliminate unwanted noise and artifact peaks. The loss or gain of a proton was corrected in negative and positive ESI modes, respectively, followed by putative identification of metabolites by accurate mass within 3 parts per million mass error searching against the Kyoto Encyclopedia of Genes and Genomes (wKEGG), MetaCyc, and LIPIDMAPS databases. The identification of putative lipids was further cross-checked by comparing elution time shifts to the number of double bonds. An increase in the number of double bonds within the corresponding fatty acyl carbon number causes linear shifts in retention time (*67*, *68*).

### Semi-quantitative analysis of sphingolipid analytes

Sphingolipids were quantified using a semi-quantitative internal standard approach with most sphingolipids having a %RSD < 15%. The concentrations, in nanomolar, were calculated as a ratio of the peak areas of identified lipid analytes over the area of the corresponding internal standards. Sphingolipid concentrations were normalized to protein levels and dried tissue weights where appropriate. The quantitation was performed using a semi-quantitative workflow on the TraceFinder 3.2 application (Thermo Fisher Scientific).

### Lipidomic data visualization

A comprehensive analysis of untargeted lipidomic data was conducted, involving data filtration, normalization, and statistical analysis. The one-factor statistical analysis method from the MetaboAnalyst software was used (*69*). To enhance the quality of analysis, variables were eliminated with relative SDs exceeding 25%, deeming them noninformative. In addition, features with more than 50% missing values were excluded from the analysis. Data were further improved by applying a series of transformations. First, a logarithmic transformation was conducted, followed by median normalization and auto scaling, which involved dividing the centered mean by the standard deviation. To visualize the distributions of lipid class concentrations, heat maps using the heatmap.2 R package were created after calculating z-score values for the normalized concentrations (https://rdrr.io/cran/gplots/man/heatmap.2.html).

### Human lymph collection

The human lymph collection was undertaken with prior written and informed consent under ethical approval from the New Zealand National Health and Disability Ethics Committee (12/NTB/67). The lymph collection for this specific lipidomic analysis was for "patient #4" as described by Escott *et al.* (*27*). Briefly, thoracic lymph sampling was performed before and throughout a stepwise increase in enteral feeding rate in human patient undergoing an Ivor Lewis oesophogastrectomy. Thoracic lymph fluid was collected every 12 hours for 5 days after surgery (*27*). Matched arterial serum samples were also collected as the lymph sampling was undertaken. The patient received Nutrison standard enteral feed (1.0 kcal/ml; 16% energy from

protein, 49% energy from carbohydrates, 35% energy from fat; Nutricia, New Zealand; https://nutricia.com.au/adult/product/nutrison/#) delivered using a standard clinical feeding pump via the patient's jejunostomy. The patient samples subsequently underwent analysis using an AbsoluteIDQ p400 kit (Biocrates Life Sciences, Innsbruck, Austria).

### Combined direct flow injection and LC-MS/MS compound identification and quantification of human thoracic lymph

We have applied a targeted quantitative metabolomics approach to analyze the serum samples using a combination of direct injection MS (AbsoluteIDQ P 400 kit) with the LC-MS/MS Kit. The kit is a commercially available assay from Biocrates Life Sciences AG (Austria). This kit, in combination with a Thermo Fisher Scientific Q-Exactive HF mass spectrometer, can be used for the targeted identification and quantification of up to 408 different endogenous metabolites including amino acids, acylcarnitines, biogenic amines, glycerophospholipids, sphingolipids, diglycerides, triglycerides, cholesteryl esters, and sugars. The method used combines the derivatization and extraction of analytes, as well as the selective mass spectrometric detection using multiple reaction monitoring pairs. Isotope-labeled internal standards and other internal standards are integrated in a kit plate filter for metabolite quantification. The AbsoluteIDQ kit contains a 96-deep-well plate with a filter plate attached with a sealing tape, and reagents and solvents used to prepare the plate assay. First 14 wells in the kit were used for one blank, three zero samples, seven standards, and three quality control samples provided with each kit. All the serum samples were analyzed with the AbsoluteIDQ Kit using the protocol described in the AbsoluteIDQ user manual. Briefly, serum samples were thawed on ice and were vortexed and centrifuged at 13,000*g*. A 10 μl of each serum sample was loaded onto the center of the filter on the upper 96-well kit plate and dried in a stream of nitrogen. Subsequently, 20 μl of a 5% solution of phenyl-isothiocyanate was added for derivatization. After incubation, the filter spots were dried again using an evaporator. The extraction of the metabolites was then achieved by adding 300 μl of methanol containing 5 mM ammonium acetate. The extracts were obtained by centrifugation into the lower 96-deep-well plate, followed by a dilution step with kit MS running solvent. Mass spectrometric analysis was performed on a Thermo Fisher Scientific Q-Exactive HF mass spectrometer equipped with a solvent delivery system. The samples were delivered to the mass spectrometer by an LC method followed by a direct injection method. The Biocrates MetIQ software was used to control the entire assay workflow from sample registration to automated calculation of metabolite concentrations to the export of data into other data analysis programs. A targeted profiling scheme was used to quantitatively screen for known small-molecule metabolites using multiple reaction monitoring, neutral loss, and precursor ion scans.

### Statistical analysis

Statistics were performed using GraphPad Prism (v9.3.1, GraphPad Software). Data are presented as means ± SEM. For statistical analysis of individual sphingolipid species between diet groups, a Student's *t* test was used for statistical comparisons. A *P* value less than 0.05 was considered statistically significant.

## Supplementary Materials

**This PDF file includes:**

Figs. S1 to S7
Tables S1 and S2

## REFERENCES AND NOTES


1. S. M. Turpin, H. T. Nicholls, D. M. Willmes, A. Mourier, S. Brodesser, C. M. Wunderlich, J. Mauer, E. Xu, P. Hammerschmidt, H. S. Brönneke, A. Trifunovic, G. LoSasso, F. T. Wunderlich, J.-W. Kornfeld, M. Blüher, M. Krönke, J. C. Brüning, Obesity-induced CerS6-dependent $C_{16:0}$ ceramide production promotes weight gain and glucose intolerance. *Cell Metab.* **20**, 678–686 (2014).
2. S. M. Turpin-Nolan, P. Hammerschmidt, W. Chen, A. Jais, K. Timper, M. Awazawa, S. Brodesser, J. C. Brüning, CerS1-derived $C_{18:0}$ ceramide in skeletal muscle promotes obesity-induced insulin resistance. *Cell Rep.* **26**, 1–10.e7 (2019).
3. W. L. Holland, J. T. Brozinick, L.-P. Wang, E. D. Hawkins, K. M. Sargent, Y. Liu, K. Narra, K. L. Hoehn, T. A. Knotts, A. Siesky, D. H. Nelson, S. K. Karathanasis, G. K. Fontenot, M. J. Birnbaum, S. A. Summers, Inhibition of ceramide synthesis ameliorates glucocorticoid-, saturated-fat-, and obesity-induced insulin resistance. *Cell Metab.* **5**, 167–179 (2007).
4. B. Chaurasia, T. S. Tippetts, R. M. Monibas, J. Liu, Y. Li, L. Wang, J. L. Wilkerson, C. R. Sweeney, R. F. Pereira, D. H. Sumida, J. A. Maschek, J. E. Cox, V. Kaddai, G. I. Lancaster, M. M. Siddique, A. Poss, M. Pearson, S. Satapati, H. Zhou, D. G. McLaren, S. F. Previs, Y. Chen, Y. Qian, A. Petrov, M. Wu, X. Shen, J. Yao, C. N. Nunes, A. D. Howard, L. Wang, M. D. Erion, J. Rutter, W. L. Holland, D. E. Kelley, S. A. Summers, Targeting a ceramide double bond improves insulin resistance and hepatic steatosis. *Science* **365**, 386–392 (2019).
5. M. Mah, M. Febbraio, S. Turpin-Nolan, Circulating ceramides—Are origins important for sphingolipid biomarkers and treatments? *Front. Endocrinol.* **12**, 684448 (2021).
6. W. L. Holland, S. A. Summers, Sphingolipids, insulin resistance, and metabolic disease: New insights from *in Vivo* manipulation of sphingolipid metabolism. *Endocr. Rev.* **29**, 381–402 (2008).
7. S. M. Turpin-Nolan, J. C. Brüning, The role of ceramides in metabolic disorders: When size and localization matters. *Nat. Rev. Endocrinol.* **16**, 224–233 (2020).
8. J. Boon, A. J. Hoy, R. Stark, R. D. Brown, R. C. Meex, D. C. Henstridge, S. Schenk, P. J. Meikle, J. F. Horowitz, B. A. Kingwell, C. R. Bruce, M. J. Watt, Ceramides contained in LDL are elevated in type 2 diabetes and promote inflammation and skeletal muscle insulin resistance. *Diabetes* **62**, 401–410 (2013).
9. P. Hammerschmidt, D. Ostkotte, H. Nolte, M. J. Gerl, A. Jais, H. L. Brunner, H.-G. Sprenger, M. Awazawa, H. T. Nicholls, S. M. Turpin-Nolan, T. Langer, M. Krüger, B. Brügger, J. C. Brüning, CerS6-derived sphingolipids interact with Mff and promote mitochondrial fragmentation in obesity. *Cell* **177**, 1536–1552.e23 (2019).
10. J. M. Adams II, T. Pratipanawatr, R. Berria, E. Wang, R. A. DeFronzo, M. C. Sullards, L. J. Mandarino, Ceramide content is increased in skeletal muscle from obese insulin-resistant humans. *Diabetes* **53**, 25–31 (2004).
11. B. C. Bergman, J. T. Brozinick, A. Strauss, S. Bacon, A. Kerege, H. H. Bui, P. Sanders, P. Siddall, T. Wei, M. K. Thomas, M. S. Kuo, L. Perreault, Muscle sphingolipids during rest and exercise: A C18:0 signature for insulin resistance in humans. *Diabetologia* **59**, 785–798 (2016).
12. C. Jiang, C. Xie, F. Li, L. Zhang, R. G. Nichols, K. W. Krausz, J. Cai, Y. Qi, Z.-Z. Fang, S. Takahashi, N. Tanaka, D. Desai, S. G. Amin, I. Albert, A. D. Patterson, F. J. Gonzalez, Intestinal farnesoid X receptor signaling promotes nonalcoholic fatty liver disease. *J. Clin. Invest.* **125**, 386–402 (2015).
13. J. Iqbal, M. M. Hussain, Intestinal lipid absorption. *Am. J. Physiol. Endocrinol. Metab.* **296**, E1183–E1194 (2009).
14. H. Vesper, E. M. Schmelz, M. N. Nikolova-Karakashian, D. L. Dillehay, D. V. Lynch, A. H. Merrill, Sphingolipids in food and the emerging importance of sphingolipids to nutrition. *J. Nutr.* **129**, 1239–1250 (1999).
15. S. Yamashita, M. Kinoshita, T. Miyazawa, Dietary sphingolipids contribute to health via intestinal maintenance. *Int. J. Mol. Sci.* **22**, 7052 (2021).
16. A. Nilsson, Metabolism of sphingomyelin in the intestinal tract of the rat. *Biochim. Biophys. Acta* **164**, 575–584 (1968).
17. E.-M. Schmelz, K. J. Crall, R. Larocque, D. L. Dillehay, A. H. Merrill, Uptake and metabolism of sphingolipids in isolated intestinal loops of mice. *J. Nutr.* **124**, 702–712 (1994).
18. E. L. Johnson, S. L. Heaver, J. L. Waters, B. I. Kim, A. Bretin, A. L. Goodman, A. T. Gewirtz, T. S. Worgall, R. E. Ley, Sphingolipids produced by gut bacteria enter host metabolic pathways impacting ceramide levels. *Nat. Commun.* **11**, 2471 (2020).
19. Y. Li, B. Chaurasia, M. M. Rahman, V. Kaddai, J. A. Maschek, J. A. Berg, J. L. Wilkerson, Z. S. Mahmassani, J. Cox, P. Wei, P. J. Meikle, D. Atkinson, L. Wang, A. M. Poss, M. C. Playdon, T. S. Tippetts, E. M. Mousa, K. Nittayaboon, P. V. A. Babu, M. J. Drummond, H. Clevers, J. A. Shayman, Y. Hirabayashi, W. L. Holland, J. Rutter, B. A. Edgar, S. A. Summers, Ceramides increase fatty acid utilization in intestinal progenitors to enhance stemness and increase tumor risk. *Gastroenterology* **165**, 1136–1150 (2023).
20. G. J. Randolph, N. E. Miller, Lymphatic transport of high-density lipoproteins and chylomicrons. *J. Clin. Invest.* **124**, 929–935 (2014).
21. Y. Li, R. J. Nicholson, S. A. Summers, Ceramide signaling in the gut. *Mol. Cell. Endocrinol.* **544**, 111554 (2022).

22. P. Wood, K. Imaichi, J. Knowles, G. Michaels, L. Kinsell, The lipid composition of human plasma chylomicrons. *J. Lipid Res.* **5**, 225–231 (1964).
23. R. Fraser, Size and lipid composition of chylomicrons of different Svedberg units of flotation. *J. Lipid Res.* **11**, 60–65 (1970).
24. C. M. Mansbach, S. A. Siddiqi, The Biogenesis of Chylomicrons. *Annu. Rev. Physiol.* **72**, 315–333 (2010).
25. F. Jeffery, T. G. Redgrave, Chylomicron catabolism differs between Hooded and albino laboratory rats. *J. Lipid Res.* **23**, 154–160 (1982).
26. L. Y. Yang, A. Kuksis, J. J. Myher, H. Pang, Surface components of chylomicrons from rats fed glyceryl or alkyl esters of fatty acids: Minor components. *Lipids* **27**, 613–618 (1992).
27. A. B. J. Escott, J. Hong, B. N. Connor, K. L. Phang, A. H. Holden, A. R. J. Phillips, J. A. Windsor, Sampling thoracic duct lymph after esophagectomy: A pilot study investigating the "gut-lymph" concept. *Lymphat. Res. Biol.* **20**, 260–274 (2022).
28. G. Gracia, E. Cao, A. P. R. Johnston, C. J. H. Porter, N. L. Trevaskis, Organ-specific lymphatics play distinct roles in regulating HDL trafficking and composition. *Am. J. Physiol. Gastrointest. Liver Physiol.* **318**, G725–G735 (2020).
29. N. L. Trevaskis, G. Lee, A. Escott, K. L. Phang, J. Hong, E. Cao, K. Katneni, S. A. Charman, S. Han, W. N. Charman, A. R. J. Phillips, J. A. Windsor, C. J. H. Porter, Intestinal lymph flow, and lipid and drug transport scale allometrically from pre-clinical species to humans. *Front. Physiol.* **11**, 458 (2020).
30. K. Kurek, D. M. Piotrowska, P. Wiesiołek-Kurek, B. Łukaszuk, A. Chabowski, J. Górski, M. Zendzian-Piotrowska, Inhibition of ceramide de novo synthesis reduces liver lipid accumulation in rats with nonalcoholic fatty liver disease. *Liver Int.* **34**, 1074–1083 (2014).
31. M. J. Watt, A. C. Barnett, C. R. Bruce, S. Schenk, J. F. Horowitz, A. J. Hoy, Regulation of plasma ceramide levels with fatty acid oversupply: Evidence that the liver detects and secretes de novo synthesised ceramide. *Diabetologia* **55**, 2741–2746 (2012).
32. M. Jiang, C. Li, Q. Liu, A. Wang, M. Lei, Inhibiting ceramide synthesis attenuates hepatic steatosis and fibrosis in rats with Non-alcoholic fatty liver disease. *Front. Endocrinol.* **10**, 665 (2019).
33. L. Sambolín-Escobales, L. Tirado-Castro, C. Suarez, D. Pacheco-Cruz, W. Fonseca-Ferrer, P. Deme, N. Haughey, G. Chompre, J. T. Porter, High-fat diet and short-term unpredictable stress increase long-chain ceramides without enhancing behavioral despair. *Front. Mol. Biosci.* **9**, 859760 (2022).
34. P. Hammerschmidt, S. M. Steculorum, C. L. Bandet, A. Del Río-Martín, L. Steuernagel, V. Kohlhaas, M. Feldmann, L. Varela, A. Majcher, M. Quatorze Correia, R. F. U. Klar, C. A. Bauder, E. Kaya, M. Porniece, N. Biglari, A. Sieben, T. L. Horvath, T. Hornemann, S. Brodesser, J. C. Brüning, CerS6-dependent ceramide synthesis in hypothalamic neurons promotes ER/mitochondrial stress and impairs glucose homeostasis in obese mice. *Nat. Commun.* **14**, 7824 (2023).
35. K. M. Boini, C. Zhang, M. Xia, J. L. Poklis, P.-L. Li, Role of sphingolipid mediator ceramide in obesity and renal injury in mice fed a high-fat diet. *J. Pharmacol. Exp. Ther.* **334**, 839–846 (2010).
36. C. Shah, G. Yang, I. Lee, J. Bielawski, Y. A. Hannun, F. Samad, Protection from high fat diet-induced increase in ceramide in mice lacking plasminogen activator inhibitor 1. *J. Biol. Chem.* **283**, 13538–13548 (2008).
37. C. Mardare, K. Krüger, G. Liebisch, M. Seimetz, A. Couturier, R. Ringseis, J. Wilhelm, N. Weissmann, K. Eder, F.-C. Mooren, Endurance and resistance training affect high fat diet-induced increase of ceramides, inflammasome expression, and systemic inflammation in mice. *J. Diabetes Res.* **2016**, 4536470 (2016).
38. A. Zalewska, M. Maciejczyk, J. Szulimowska, M. Imierska, A. Błachnio-Zabielska, High-fat diet affects ceramide content, disturbs mitochondrial redox balance, and induces apoptosis in the submandibular glands of mice. *Biomolecules* **9**, 877 (2019).
39. J. M. Haus, S. R. Kashyap, T. Kasumov, R. Zhang, K. R. Kelly, R. A. DeFronzo, J. P. Kirwan, Plasma ceramides are elevated in obese subjects with type 2 diabetes and correlate with the severity of insulin resistance. *Diabetes* **58**, 337–343 (2009).
40. L. Wigger, C. Cruciani-Guglielmacci, A. Nicolas, J. Denom, N. Fernandez, F. Fumeron, P. Marques-Vidal, A. Ktorza, W. Kramer, A. Schulte, H. Le Stunff, R. Liechti, I. Xenarios, P. Vollenweider, G. Waeber, I. Uphues, R. Roussel, C. Magnan, M. Ibberson, B. Thorens, Plasma dihydroceramides are diabetes susceptibility biomarker candidates in mice and humans. *Cell Rep.* **18**, 2269–2279 (2017).
41. J. W. Meeusen, L. J. Donato, S. C. Bryant, L. M. Baudhuin, P. B. Berger, A. S. Jaffe, Plasma ceramides: A novel predictor of major adverse cardiovascular events after coronary angiography. *Arterioscler. Thromb. Vasc. Biol.* **38**, 1933–1939 (2018).
42. M. Hilvo, T. Salonurmi, A. S. Havulinna, D. Kauhanen, E. R. Pedersen, G. S. Tell, K. Meyer, A.-M. Teeriniemi, T. Laatikainen, P. Jousilahti, M. J. Savolainen, O. Nygård, V. Salomaa, R. Laaksonen, Ceramide stearic to palmitic acid ratio predicts incident diabetes. *Diabetologia* **61**, 1424–1434 (2018).
43. Y. Kim, G. Volpert, K. Shin, S. Kim, S. Shin, Y. Lee, S. H. Sung, Y. Lee, J. Ahn, Y. Pewzner-Jung, W. Park, A. H. Futerman, J. Park, Ablation of ceramide synthase 2 exacerbates dextran sodium sulphate-induced colitis in mice due to increased intestinal permeability. *J. Cell. Mol. Med.* **21**, 3565–3578 (2017).
44. Z. Li, I. Kabir, G. Tietelman, C. Huan, J. Fan, T. Worgall, X.-C. Jiang, Sphingolipid de novo biosynthesis is essential for intestine cell survival and barrier function. *Cell Death Dis.* **9**, 1–13 (2018).
45. C. Xie, C. Jiang, J. Shi, X. Gao, D. Sun, L. Sun, T. Wang, S. Takahashi, M. Anitha, K. W. Krausz, A. D. Patterson, F. J. Gonzalez, An Intestinal farnesoid X receptor–ceramide signaling axis modulates hepatic gluconeogenesis in mice. *Diabetes* **66**, 613–626 (2017).
46. X. Wang, Y. Wang, J. Xu, C. Xue, Sphingolipids in food and their critical roles in human health. *Crit. Rev. Food Sci. Nutr.* **61**, 462–491 (2021).
47. M. Le Barz, C. Vors, E. Combe, L. Joumard-Cubizolles, M. Lecomte, F. Joffre, M. Trauchessec, S. Pesenti, E. Loizon, A.-E. Breyton, E. Meugnier, K. Bertrand, J. Drai, C. Robert, A. Durand, C. Cuerq, P. Gaborit, N. Leconte, A. Bernalier-Donadille, E. Cotte, M. Laville, S. Lambert-Porcheron, L. Ouchchane, H. Vidal, C. Malpuech-Brugère, D. Cheillan, M.-C. Michalski, Milk polar lipids favorably alter circulating and intestinal ceramide and sphingomyelin species in postmenopausal women. *JCI Insight* **6**, e146161 (2021).
48. J. Y. Xia, W. L. Holland, C. M. Kusminski, K. Sun, A. X. Sharma, M. J. Pearson, A. J. Sifuentes, J. G. McDonald, R. Gordillo, P. E. Scherer, Targeted induction of ceramide degradation leads to improved systemic metabolism and reduced hepatic steatosis. *Cell Metab.* **22**, 266–278 (2015).
49. N. Turner, G. M. Kowalski, S. J. Leslie, S. Risis, C. Yang, R. S. Lee-Young, J. R. Babb, P. J. Meikle, G. I. Lancaster, D. C. Henstridge, P. J. White, E. W. Kraegen, A. Marette, G. J. Cooney, M. A. Febbraio, C. R. Bruce, Distinct patterns of tissue-specific lipid accumulation during the induction of insulin resistance in mice by high-fat feeding. *Diabetologia* **56**, 1638–1648 (2013).
50. A. H. Merrill, S. Lingrell, E. Wang, M. Nikolova-Karakashian, T. R. Vales, D. E. Vance, Sphingolipid biosynthesis de novo by rat hepatocytes in culture. Ceramide and sphingomyelin are associated with, but not required for, very low density lipoprotein secretion. *J. Biol. Chem.* **270**, 13834–13841 (1995).
51. J. Ishikawa, S. Takada, K. Hashizume, Y. Takagi, M. Hotta, Y. Masukawa, T. Kitahara, Y. Mizutani, Y. Igarashi, Dietary glucosylceramide is absorbed into the lymph and increases levels of epidermal sphingolipids. *J. Dermatol. Sci.* **56**, 216–218 (2009).
52. T. Sugawara, T. Tsuduki, S. Yano, M. Hirose, J. Duan, K. Aida, I. Ikeda, T. Hirata, Intestinal absorption of dietary maize glucosylceramide in lymphatic duct cannulated rats. *J. Lipid Res.* **51**, 1761–1769 (2010).
53. M. Morifuji, S. Higashi, C. Oba, S. Ichikawa, K. Kawahata, T. Yamaji, H. Itoh, Y. Manabe, T. Sugawara, Milk phospholipids enhance lymphatic absorption of dietary sphingomyelin in lymph-cannulated rats. *Lipids* **50**, 987–996 (2015).
54. N. Tomonaga, T. Tsuduki, Y. Manabe, T. Sugawara, Sphingoid bases of dietary ceramide 2-aminoethylphosphonate, a marine sphingolipid, absorb into lymph in rats. *J. Lipid Res.* **60**, 333–340 (2019).
55. B. Vergès, Intestinal lipid absorption and transport in type 2 diabetes. *Diabetologia* **65**, 1587–1600 (2022).
56. G. F. Lewis, K. Uffelman, M. Naples, L. Szeto, M. Haidari, K. Adeli, Intestinal lipoprotein overproduction, a newly recognized component of insulin resistance, is ameliorated by the insulin sensitizer rosiglitazone: studies in the fructose-fed Syrian golden hamster. *Endocrinology* **146**, 247–255 (2005).
57. C.-M. Lo, B. K. Nordskog, A. M. Nauli, S. Zheng, S. B. vonLehmden, Q. Yang, D. Lee, L. L. Swift, N. O. Davidson, P. Tso, Why does the gut choose apolipoprotein B48 but not B100 for chylomicron formation? *Am. J. Physiol. Gastrointest. Liver Physiol.* **294**, G344–G352 (2008).
58. E. Cao, M. J. Watt, C. J. Nowell, T. Quach, J. S. Simpson, V. De Melo Ferreira, S. Agarwal, H. Chu, A. Srivastava, D. Anderson, G. Gracia, A. Lam, G. Segal, J. Hong, L. Hu, K. L. Phang, A. B. J. Escott, J. A. Windsor, A. R. J. Phillips, D. J. Creek, N. L. Harvey, C. J. H. Porter, N. L. Trevaskis, Mesenteric lymphatic dysfunction promotes insulin resistance and represents a potential treatment target in obesity. *Nat. Metab.* **3**, 1175–1188 (2021).
59. J. Hong, S. Nachkebia, S. M. Tun, A. Petzer, J. A. Windsor, A. J. Hickey, A. R. Phillips, Altered metabolic profile of triglyceride-rich lipoproteins in gut-lymph of rodent models of sepsis and gut ischemia-reperfusion injury. *Dig. Dis. Sci.* **63**, 3317–3328 (2018).
60. S. Reißig, C. Hackenbruch, N. Hövelmeyer, Isolation of T cells from the gut. *Methods Mol. Biol.* **1193**, 21–25 (2014).
61. J. Schwamb, V. Feldhaus, M. Baumann, M. Patz, S. Brodesser, R. Brinker, J. Claasen, C. P. Pallasch, M. Hallek, C.-M. Wendtner, L. P. Frenzel, B-cell receptor triggers drug sensitivity of primary CLL cells by controlling glucosylation of ceramides. *Blood* **120**, 3978–3985 (2012).
62. N. L. Trevaskis, L. Hu, S. M. Caliph, S. Han, C. J. H. Porter, The mesenteric lymph duct cannulated rat model: Application to the assessment of intestinal lymphatic drug transport. *J. Vis. Exp.* **97**, e52389 (2015).
63. A. L. Ostermann, C. M. Wunderlich, L. Schneiders, M. C. Vogt, M. A. Woeste, B. F. Belgardt, C. M. Niessen, B. Martiny, A. C. Schauss, P. Frommolt, A. Nikolaev, N. Hövelmeyer, R. C. Sears, P. J. Koch, D. Günzel, J. C. Brüning, F. T. Wunderlich, Intestinal insulin/IGF1 signalling through FoxO1 regulates epithelial integrity and susceptibility to colon cancer. *Nat. Metab.* **1**, 371–389 (2019).

64. Z. H. Alshehry, C. K. Barlow, J. M. Weir, Y. Zhou, M. J. McConville, P. J. Meikle, An Efficient Single Phase Method for the Extraction of Plasma Lipids. *Metabolites* **5**, 389–403 (2015).
65. K. Yeshi, D. J. Creek, D. Anderson, E. Ritmejerytė, L. Becker, A. Loukas, P. Wangchuk, Metabolomes and Lipidomes of the Infective Stages of the *Gastrointestinal nematodes*, *Nippostrongylus brasiliensis* and *Trichuris muris*. *Metabolites* **10**, 446 (2020).
66. D. J. Creek, A. Jankevics, K. E. V. Burgess, R. Breitling, M. P. Barrett, IDEOM: an Excel interface for analysis of LC–MS-based metabolomics data. *Bioinformatics*, **28**, 1048–1049 (2012). https://doi.org/10.1093/bioinformatics/bts069.
67. A. Fauland, H. Köfeler, M. Trötzmüller, A. Knopf, J. Hartler, A. Eberl, C. Chitraju, E. Lankmayr, F. Spener, A comprehensive method for lipid profiling by liquid chromatography-ion cyclotron resonance mass spectrometry. *J. Lipid Res.* **52**, 2314–2322 (2011).
68. J. B. White, P. J. Trim, T. Salagaras, A. Long, P. J. Psaltis, J. W. Verjans, M. F. Snel, Equivalent carbon number and interclass retention time conversion enhance lipid identification in untargeted clinical lipidomics. *Anal. Chem.* **94**, 3476–3484 (2022).
69. Z. Pang, J. Chong, S. Li, J. Xia, MetaboAnalystR 3.0: Toward an Optimized Workflow for Global Metabolomics. *Metabolites* **10**, 186 (2020).

**Acknowledgments:** We acknowledge the work of the staff at the animal research facilities at Monash Institute of Pharmaceutical Sciences, Monash University. We also acknowledge the contribution of C. Egan and E. McLennan for the technical expertise in rodent handling and contribution to this dataset. We acknowledge the contribution of J. C. Brüning of the Max Planck Institute for Metabolism Research, Cologne, Germany, for access to high-fat diet animal tissues that contributed to this dataset. **Funding:** M.A.F. is a Senior Principal Research Fellow of the NHMRC (APP1116936) and is also supported by an NHMRC Investigator Grant (APP1194141). Research in his laboratory was supported by project grants from the NHMRC (APP1042465, APP1041760, APP1156511, and APP1122227 to M.A.F.). J.H., J.A.W., and A.R.J.P. were supported by The Health Research Council of New Zealand (grant number: 15/30) and the Maurice and Phyllis Paykel Trust (grant number: 3706308), which funded the human lymph sample collection and analysis. S.M.T.-N. received grant support for the preliminary animal study by CECAD, Cologne, Germany (CECAD Senior Postdoctoral Fellow Research Grant 2016). S.M.T.-N., N.L.T., C.Z., and D.J.C. received grant support for the rat cannulation study by Monash University, Australia (JMP19-0040). S.M.T.-N. was supported by a REDI Fellowship, MRFF–NHMRC (REDI274). **Author contributions:** Conceptualization: S.M.T.-N., N.L.T., C.Z., D.J.C., and M.A.F. Methodology: M.S.M.M., S.M.T.-N., E.C., G.G., J.S., S.B., J.H., J.A.W., A.R.J.P., and N.L.T. Investigation: M.S.M.M. and S.M.T.-N. Analysis: M.S.M.M., S.M.T.-N., S.T., D.A., A.E., and S.B. Bioinformatics: S.T. Supervision: S.M.T.-N., M.A.F., and N.L.T. Writing—original draft: M.S.M.M., M.AF., S.M.T.-N. Writing—review and editing: All authors. Funding acquisition: S.M.T.-N., N.L.T., C.Z., D.J.C., J.W., A.R.J.P., and M.A.F. **Competing interests:** M.A.F. holds a U.S. patent no. 20200179363 methods for treating Nonalcoholic steatohepatitis (NASH) and for preventing NASH-induced hepatocellular carcinoma (HCC). M.A.F. is a shareholder and scientific advisor for N-Gene Pharmaceuticals. M.A.F. is the founder and shareholder of Celesta Therapeutics. N.L.T. is an inventor of a lymph-directing glyceride prodrug technology that has been patented and licensed via a commercial agreement with PureTech Health. PureTech Health has subsequently entered into a collaboration agreement with Boehringer Ingelheim to explore the technology in immune modulation. N.L.T. also currently has research funding from Protagonist and Moderna to evaluate lymphatic delivery. N.L.T. is an inventor of a lymph-directing glyceride prodrug technology (PCT/AU2020/050997). This technology has been patented and licensed via a commercial agreement with PureTech Health and Seaport Therapeutics. N.L.T. has consulted with the following companies: Amgen, AstraZeneca, Biolingus, BioNTech, Eli Lilly, Genentech, Janssen, Merck, Moderna, Novartis, Noxopharm, Pfizer, Protagonist, and Puretech Health. All other authors declare that they have no competing interests. **Data and materials availability:** All data needed to evaluate the conclusions in the paper are present in the paper and/or the Supplementary Materials.

Submitted 13 March 2024
Accepted 19 July 2024
Published 23 August 2024
10.1126/sciadv.adp2254